

Dynamical localization in microdisk lasers

W. Fang^{1*}, H. Cao¹, V. A. Podolskiy^{2,3}, and E. E. Narimanov²

¹ Department of Physics and Astronomy, Northwestern University, Evanston, IL 60208

² Electrical Engineering Department, Princeton University, Princeton, NJ 08544

³ Physics Department, Oregon State University, Corvallis, OR 97331

w-fang@northwestern.edu; VP:vpodolsk@physics.orst.edu;

evgenii@princeton.edu; h-cao@northwestern.edu

<http://www.physics.northwestern.edu/Cao/>

<http://www.physics.orst.edu/~vpodolsk>; <http://www.ee.princeton.edu/~evgenii>

Abstract: We demonstrate the lasing action from a dynamically localized mode in a microdisk resonator with rough boundary. Although substantial boundary roughness and surface defects in our devices imply strong light scattering and destroy the regular whispering gallery modes, the destructive interference of the scattered light leads to the dynamical Anderson localization in the phase space of the system and the formation of a different type of high- Q modes. Using direct optical imaging of the lasing mode and theoretical calculations, we show that the lasing modes in our devices has dynamical localization origin. This behavior, although demonstrated here in GaAs-InAs microdisk laser, should be applicable to any lasers and sensors based on semiconductor or polymer materials.

© 2005 Optical Society of America

OCIS codes: (140.3410) Laser resonators; (140.1540) Chaos.

References and links

1. S.X. Qian, J. Snow, H.M. Tzeng & R.K. Chang, "Lasing droplets - highlighting the liquid-air interface by laser-emission," *Science* **231**, 486-488 (1986).
2. K. Djordjev, S. Choi, S. Choi, and P. Dapkus, "High-Q vertically coupled InP microdisk resonators," *IEEE Photonics Technol. Lett.* **14**, 331-333 (2002).
3. B. Gayral, J. M. Gerard, A. Lemaitre, C. Dupuis, L. Manin, and J. L. Pelouard, "High-Q wet-etched GaAs microdisks containing InAs quantum boxes," *Appl. Phys. Lett.* **75**, 1908-1910 (1999).
4. B. Corbett, J. Justice, L. Considine, S. Walsh, W.M. Kelly, "Low-threshold lasing in novel microdisk geometries," *IEEE Photonics Technol. Lett.* **8**, 855-857 (1996).
5. T. Kipp, L. Rolf, C. Schuller, D. Endler, Ch. Heyn, and D. Heitmann, "Selectively enhanced inelastic light scattering of electronic excitations in a semiconductor microcavity," *Phys. Rev. B* **63**, 195304 (2001).
6. J. U. Nöckel, A. D. Stone, G. Chen, H. Grossman and R. K. Chang, "Directional emission from asymmetric resonant cavities," *Opt. Lett.* **21**, 1609-1611 (1996).
7. E. E. Narimanov, G. Hackenbroich, P. Jacquod, and A. D. Stone, "Semiclassical theory of the emission properties of wave-chaotic resonant cavities," *Phys. Rev. Lett.* **83**, 4991-4994 (1999).
8. It can be shown that in 2D the small wavelength approximation to the solutions of Maxwell equations is essentially equivalent to the standard semiclassical limit of Schrödinger Equation.
9. J. U. Nöckel, A. D. Stone, "Ray and wave chaos in asymmetric resonant optical cavities," *Nature* **385**, 45-47 (1997).
10. K.M. Frahm and D.L. Shepelyansky, "Quantum localization in rough billiards," *Phys. Rev. Lett* **78**, 1440-1443 (1997).

11. S. L. McCall, A. F. J. Levi, R. E. Slusher, S. J. Pearton, and R. A. Logan, "Whispering-gallery mode microdisk lasers," *Appl. Phys. Lett.* **60**, 289-291 (1992).
12. M. Berry, "Regular and irregular semiclassical wavefunctions," *J. Phys. A* **10**, 2083 (1977).
13. M. Gutzwiller, *Chaos in Classical and Quantum Mechanics* (Springer-Verlag, New York, 1991).
14. G. Casati, B. V. Chirikov, J. Ford, and F. M. Izrailev, in *Stochastic Behavior in Classical and Quantum Hamiltonian Systems*, Lecture Notes in Physics Vol. **93** (Springer, Berlin, 1979), p. 334.
15. S. Fishman, D. R. Grempel, and R. E. Prange, "Chaos, quantum recurrences, and Anderson localization," *Phys. Rev. Lett.* **49**, 509-512 (1982).
16. J. Ringor, P. Szriftgiser, J. C. Carreau, D. Delande, "Experimental evidence of dynamical localization and delocalization in a quasiperiodic driven system," *Phys. Rev. Lett.* **85**, 2741-2744 (2000).
17. L. Sirko, Sz. Bauch, Y. Hlushchuk, P.M. Koch, R. Blümel, M. Barth, U. Kuhl, and H.-J. Stöckmann, "Observation of dynamical localization in a rough microwave cavity," *Phys. Lett. A* **266**, 331-335 (2000).
18. O.A. Starykh, P.R.J. Jacquod, E.E. Narimanov, and A.D. Stone, "Signature of dynamical localization in the resonance width distribution of wave-chaotic dielectric cavities," *Phys. Rev. E* **62**, 2078-2084 (2000).
19. V.A. Podolskiy, E.E. Narimanov, W. Fang, and H. Cao, "Chaotic microlasers based on dynamical localization," *Proceedings of Nat. Acad. of Sci.* **101**, 10498-10500 (2004).
20. H. Cao, J.Y. Xu, W.H. Xiang, Y. Ma, S.-H. Chang, S. T. Ho, and G.S. Solomon, "Optically pumped InAs quantum dot microdisk lasers," *Appl. Phys. Lett.* **76**, 3519-3521 (2000).
21. D. K. Armani, T. J. Kippenberg, S. M. Spillane, and K. J. Vahala, "Ultra-high-Q toroid microcavity on a chip," *Nature* **421**, 925-928 (2003).
22. G. Casati, I. Guarneri, and D. Shepelyansky, "Exponential photonic localization for the hydrogen atom in a monochromatic field," *Phys. Rev. A* **36**, 3501-3504 (1987).
23. F. Haake *Quantum Signatures of Chaos* Springer NY (2000).
24. E. Doron, U. Smilansky, "Chaotic spectroscopy," *Phys. Rev. Lett.* **68**, 1255-1258 (1992).
25. H.E. Tureci, H.G.L. Schwefel, P. Jacquod, A.D. Stone, "Modes of wave-chaotic dielectric resonators," ArXiv: physics/0308016 (2003)

1. Introduction

Due to their compact dimensions, long mode lifetime, and high versatility, semiconductor microdisk resonators are among the most suitable components for microlasers, microsensors, and micro-detectors [1, 2, 3]. The scientific and engineering aspects of these devices have therefore recently gained considerable attention [4, 5].

The mode structure of these *circular* microdisk resonators is usually associated with stable quasi-periodic whispering-gallery (WG) ray trajectories. Each such trajectory corresponds to a particular value of angular momentum, characterized by the (conserved) angle of incidence χ (see Fig. 1 a). In the quasi-classic case – when the radius of the cavity R_0 is much larger than the "internal" wavelength $\lambda = \lambda_0/n$ (n being the refraction index of the disk) – the modes of the system can be deduced from the regular trajectories via Einstein-Brillouin-Keller quantization scheme [6, 7, 8]. Since the trajectories with $\sin \chi > 1/n$ are classically trapped inside the cavity, the finite lifetime of the corresponding modes of the optical resonator is attributed to diffraction loss through the curved boundary known as evanescent escape. Since such an escape corresponds to violation of classical (ray) dynamics, it is exponentially suppressed (as any tunneling process in wave-mechanical system), giving rise to the Q-factors up to 10^5 . [3]

However, the above semiclassical ray-to-wave correspondence is based on the fact that the conserved angular momentum of the ray trajectory can be used as a "good mode number" for the wave-optical system, and thus is valid only for an ideal circular geometry. Any deviations from this ideal case – due to e.g. boundary roughness and surface defects, leading to light scattering (and correspondingly to change of the angular momentum of the trajectory), will inevitably break this idealized picture.

In particular, the symmetry of the resonator boundary is generally broken by the surface roughness, inevitable in the device fabrication. Quantitatively, the degree of roughness can be

characterized by the parameter

$$\kappa = \left\langle \left(\frac{dR}{d\phi} \right)^2 \right\rangle^{1/2} \quad (1)$$

Below the critical value of κ_c corresponding to the classical transition from integrability to chaos (whose value is not universal and depend on the functional form of the deformation $\delta R(\phi) \equiv R(\phi) - R_0$), the ray trajectories inside the cavity remain quasi-regular [see Fig. 1 (b)] and are still trapped inside by the total internal reflection. In this case, the mode patterns and lifetimes can be obtained using adiabatic approach [6, 9] assuming that the high- Q modes of the asymmetric resonator adiabatically evolve from the original WG modes of the circular resonator.

In contrast to this behavior, for $\kappa > \kappa_c$ the ray dynamics inside the cavity becomes completely chaotic, and no classical orbits are trapped inside the cavity (see Fig. 1 c).

Nevertheless, the high- Q modes can exist in the cavity even in the case $\kappa > \kappa_c$. The physical reasons behind this seeming inconsistency strongly depend on the relation between the size of the cavity and the wavelength of light inside the system. Namely, when the deviations from the idealized geometry are substantially smaller than the wavelength, they only lead to a small change in the mode patterns and lifetimes which can be calculated using perturbation theory. In this regime the high- Q modes preserve their “whispering-gallery nature”, regardless of the nature of the resulting ray dynamics in the “rough” resonator. Quantitatively [10], in rough resonators¹ the perturbative regime is observed when

$$\kappa \ll \lambda/R_0 \quad (2)$$

where $R_0 = \langle R(\phi) \rangle$ is the average of the radius of the resonator boundary $R(\phi)$. Many earlier experiments, including the pioneering work of McCall *et al* [11], probed this regime.

In contrast to this behavior, when the requirement (2) is violated and $\kappa \geq \lambda/R_0$, the (chaotic) nature of the underlying ray dynamics does strongly affect the modes of the resonator. The famous “Berry’s conjecture” [12] then implies that the modes follow the random patterns formed by chaotic ray trajectories, and behave essentially similar to random superpositions of plane waves. As Berry’s conjecture has been extensively tested for various geometries [13], one may be strongly tempted to conclude that high- Q modes in microdisk resonators can only be found for small roughness when $\kappa < \max[\lambda/R_0, \kappa_c]$ – which implies severe limitations on the fabrication tolerance of the final device performance.

However, in the mechanism known as dynamical Anderson localization (DL) [14, 15, 16], the destructive interference of the scattered light may lead to suppression of the chaotic scattering and to the formation of the modes strongly localized in the phase space. In particular, it was shown that in “rough billiards” dynamical localization may lead to exponential localization of modes in the angular momentum space [10, 17].

Although the refractive and evanescent escape from the dielectric microdisk resonator make it a different dynamical system from a point particle in a billiard with ideal reflective walls, the quasi-stationary states of the electromagnetic field in a rough optical resonator retain the dynamical localized nature which shows up in the log-normal distribution of their lifetimes[18]. By virtue of its “heavy tail” for large lifetimes, the log-normal distribution implies the existence of high- Q modes even in a microdisk resonator with strong boundary roughness. Lasing in one of these modes would therefore be a direct evidence of dynamical localization.

¹For a rough resonator, in polar coordinates the radius is defined by $R(\phi) = R_0 + \sum_{m=1}^M [a_m \cos(b_m \phi) + b_m \sin(m\phi)]$ with a finite $M \sim \lambda/R_0$

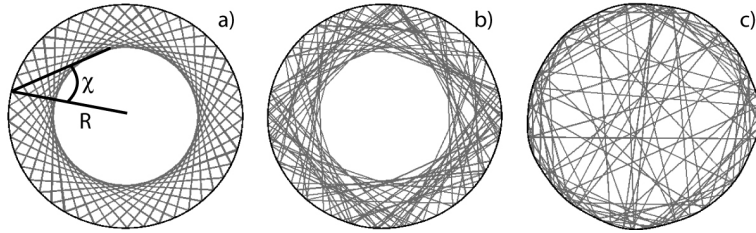


Fig. 1. The typical ray trajectory in circular (a) and rough (b, c) resonators. The resonator geometry in (b) corresponds to the adiabatic regime ($\kappa \approx 0.06$), the geometry in (c) corresponds to the device studied in our experiments ($\kappa \approx 0.2$).

In this paper we present a detailed study of lasing behavior from high- Q modes of semiconductor microdisks with rough boundary, briefly reported in Ref. [19]. We calculate the quasi-stationary states in our microdisk devices, and directly show the exponential localization of lasing modes in the angular momentum. By comparing the theoretical mode patterns with the experimental data obtained by direct optical imaging, we identify the lasing mode and confirm its dynamically localized structure.

This finding has important experimental and technological implications. First, since boundary roughness and surface defects are inevitable, the resulting high- Q modes will be different from those of the idealized circular resonator – and this should be taken into account in the device engineering and characterization. Second, the “survival” of high- Q modes in rough devices implies that for some applications one can relax the fabrication tolerance requirements for microdisk resonators.

The rest of the article is organized as follows. In the next section we present the details of our experimental setup and describe the measured results; Section 3 is devoted to theoretical confirmation of the DL mode structure; last Section presents concluding remarks.

2. Experimental results

Our dielectric microlaser is made of 200 nm thick GaAs layer with a thin InAs quantum well in the middle. The microdisks (with the typical diameter close to $5\mu\text{m}$) are fabricated by optical lithography and two-step wet etching [20]. To isolate the disks from the GaAs substrate, each disk is supported by a 500nm-long AlGaAs pedestal. As the etching process is not exactly isotropic, the shapes of the disk deviate from an ideal circle. Figure 2 shows the scanning electron microscope (SEM) images of a typical disk – note the roughness at the disk boundary revealed in the magnified image (left panel).

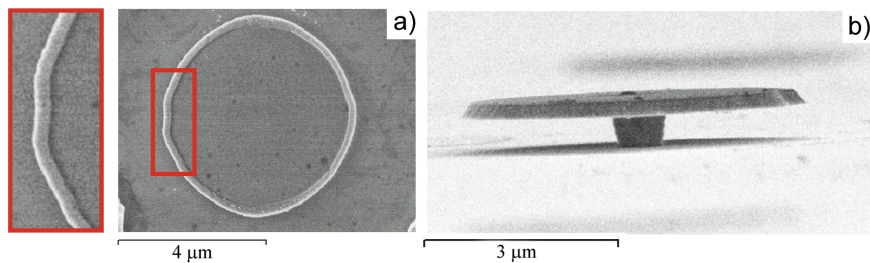


Fig. 2. Top (a) and side (b) view SEM images of a GaAs microdisk on an $\text{Al}_{0.7}\text{Ga}_{0.3}$ pedestal.

The lasing experiment is performed on individual disks. The microdisks are mounted in a low temperature cryostat, and cooled down to 10K. The InAs quantum well is optically excited by a modelocked Ti-sapphire laser at 790 nm. The pump beam is focused by an objective lens onto a single disk. The emission from the disk is collected by the same lens, and sent to a 0.5-meter spectrometer with a liquid nitrogen cooled charge coupled device (CCD) array detector. Figures 3 - 6 are the data of the measurement of the disk in Fig. 2. As shown in Fig. 3(a), the emission spectrum features a broadband amplified spontaneous emission (ASE) and several distinct peaks that correspond to the cavity modes. Figure 3(b) is a plot of the intensity and linewidth of one mode at $\lambda_0=855.5\text{nm}$ as a function of the incident pump power. When the pump power exceeds a threshold, the emission intensity exhibits a sudden increase accompanied by a simultaneous decrease of the mode linewidth. This threshold behavior corresponds to the onset of lasing oscillation in this mode. At high pumping levels, lasing may occur in several cavity modes.

To find out the spatial profile of the lasing mode, we use a bandpass filter of 1nm width to single out the mode at 855.5nm. The filtered spectrum obtained in this measurement, is shown in Fig. 4 as the solid curve. The spatial distribution of the mode intensity on the disk surface is projected onto a digital CCD camera by an objective lens. As shown in the inset I of Fig. 4, the near-field image of the lasing mode reveals its intensity is concentrated near the disk edge. Thus, the lasing mode is similar to a whispering-gallery mode, despite of the boundary roughness. We extract the spatial intensity distribution $I(r, \theta)$ from the digital image, and calculate the radial distribution by integrating over the angle:

$$I_r(r) = \frac{1}{2\pi} \int_0^{2\pi} I(r, \theta) d\theta \quad (3)$$

The data for $I_r(r)$ at several pump powers are shown in Fig. 5(a). Well below the lasing threshold, $I_r(r)$ represents the radial distribution of spontaneous emission, which is nearly constant across the disk. When the pump power approaches the lasing threshold, the contribution of the lasing mode gradually dominates the radial intensity distribution. The intensity near the disk boundary grows much faster than that in the disk center. This change in the intensity profile coincides with the rapid increase of the lasing mode intensity in the emission spectrum. An intensity maximum is developed close to the disk boundary. To confirm that the intensity maximum comes from the lasing mode, we measure the spatial distribution of the amplified spontaneous emission at the same pump power – which is obtained when the frequency of the bandpass filter is tuned away from any cavity resonance. The dashed curve in Fig. 4 shows the filtered spectrum of the ASE alone. The inset II of Fig. 4 is the corresponding near-field image. It reveals a virtually uniform distribution of the amplified spontaneous emission across the disk. The radial distribution of ASE intensity, plotted as the dashed line in Fig. 5(b), is nearly independent of r . The dramatic difference in the spatial distribution of the laser emission and the ASE indicates that the lasing mode is localized near the disk boundary.

We also measure the spectra of emission from different parts of a microdisk. We use an objective lens to project a magnified image of the microdisk onto the entrance slit of an imaging spectrometer. The magnification is about 400 times, thus the disk image is about 2mm in diameter. We first fully open the entrance slit and rotate the grating to the position of the zeroth order diffraction (i.e., reflection). The spectrometer projects the image at the plane of the entrance slit onto the two-dimensional (2D) CCD array detector mounted at the exit port. After aligning the disk image to the center of the entrance slit, we reduce the width of the entrance slit to 0.1 mm. Now only the emission from a narrow strip along the vertical diameter of the disk can enter the spectrometer. The grating is rotated back to the position of the first-order diffraction, so that the light at different wavelength is dispersed in the horizontal direction. The CCD array

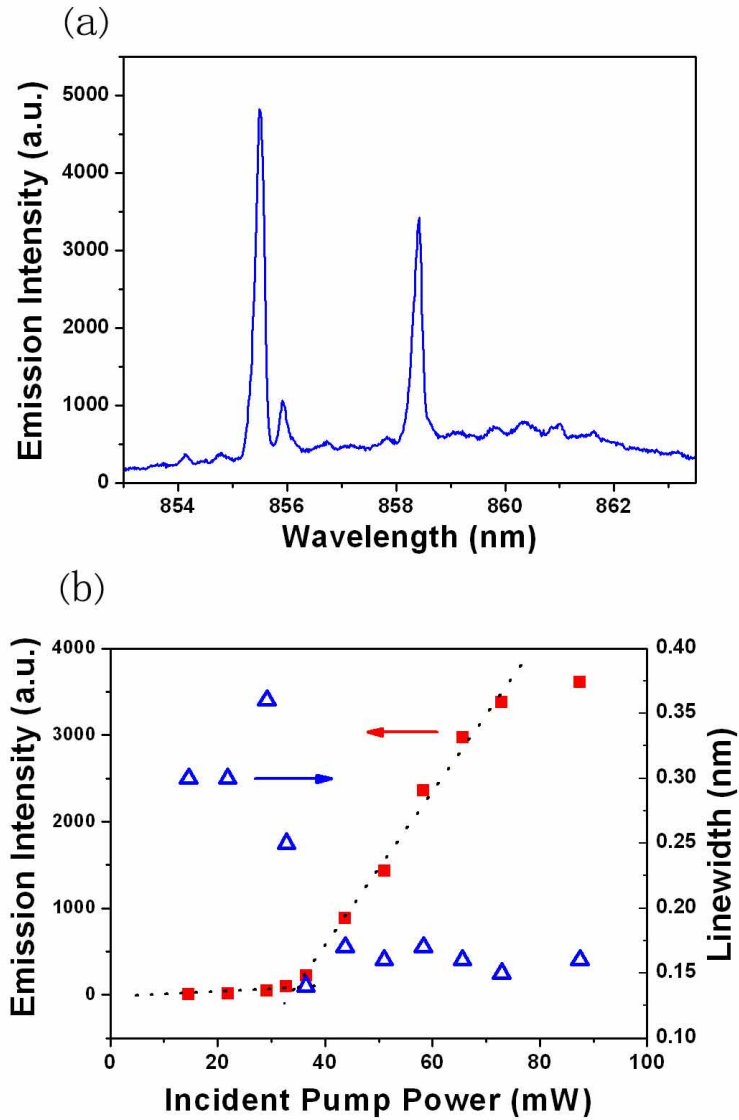


Fig. 3. (a) Spectrum of emission from the GaAs microdisk shown in Fig. 2. The incident pump power is $44\mu\text{W}$. (b) The emission intensity and linewidth of the mode at 855.5nm as a function of the incident pump power.

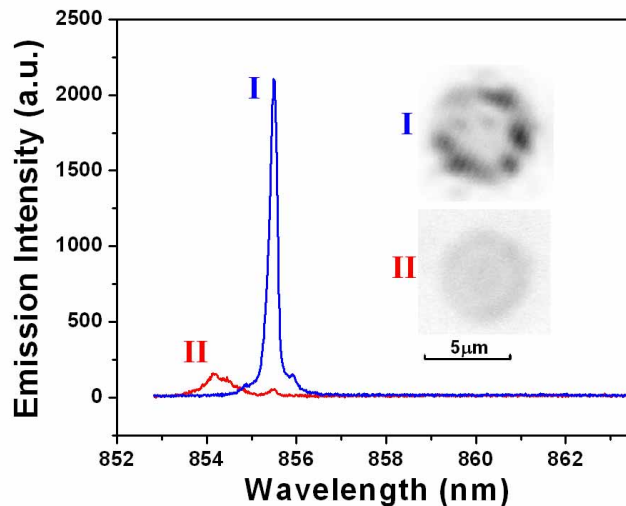


Fig. 4. The blue curve I and the inset I are the spectrum and near-field image taken when the bandpass filter is tuned to the mode at 855.5nm. The red curve II and the inset II are the spectrum and image taken when the bandpass filter is tuned away from any cavity resonance. The incident pump power is $44\mu\text{W}$.

detector, located at the image plane of the entrance slit, captures a 2D spatial-spectral image of the microdisk emission.

The resulting “local” spectral data are presented in Fig. 6. In the panel (a), each dark vertical line in the 2D image corresponds to a cavity mode. Because the vertical coordinate in Fig. 6(a) represents the spatial location on the disk, we can obtain the emission spectra from different parts of the disk by dividing the 2D image into many horizontal strips. In particular, the horizontal strip marked by 1 corresponds to the disk edge, while the strip marked by 2 is close to the disk center. The emission spectra, obtained by integrating over the spatial coordinate inside the strips 1 and 2, are shown in Fig. 6(b). In the spectrum of emission collected from the disk edge, the lasing peak at 855.5nm is much higher than the ASE background. But in the spectrum of emission taken from the disk center, the peak at 855.5nm is much weaker, although the ASE is a little stronger. Similarly, by dividing the 2D images into vertical strips and integrating over the spectral coordinate inside the strips, we can obtain the spatial distribution of emission intensity in any frequency range. For example, the vertical strip marked by α is centered at 855.5nm and has a width of 0.5 nm. It gives the spatial variation of the lasing mode intensity across the vertical diameter of the disk [Fig. 6(c)]. The lasing mode is peaked near the two ends of the disk. The vertical strip marked by β covers a frequency range that has only ASE. It gives the spatial distribution of the ASE intensity which is nearly constant across the disk diameter.

The above experimental data clearly show that in this $5\mu\text{m}$ disk with rough boundary, the lasing mode at 855.5nm has WG-like structure – its intensity near the disk boundary is much stronger than that at the disk center. We have repeated the above measurements with many lasing modes in different microdisks, and similar results are obtained.

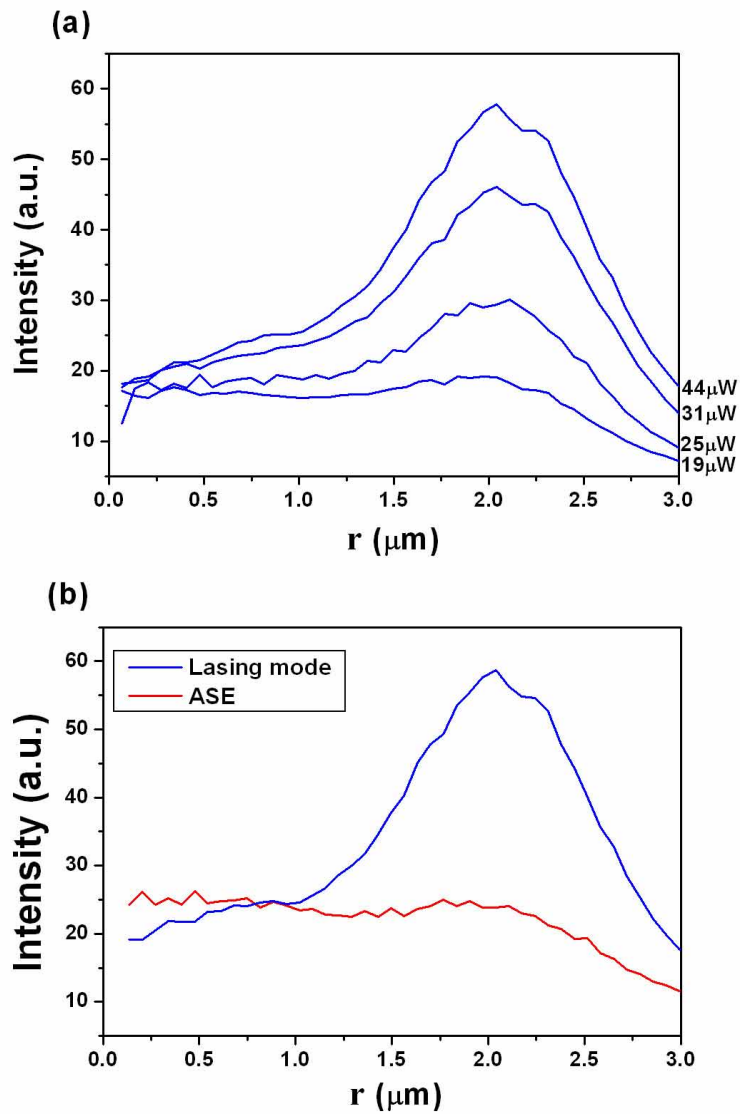


Fig. 5. (a) Radial distribution of the emission intensity when the bandpass filter is tuned to the mode at 855.5nm. The incident pump powers are marked next to the curves. (b) The blue (red) curve represents the radial distribution of the laser emission (or amplified spontaneous emission) intensity obtained from the inset I (II) in Fig. 4.

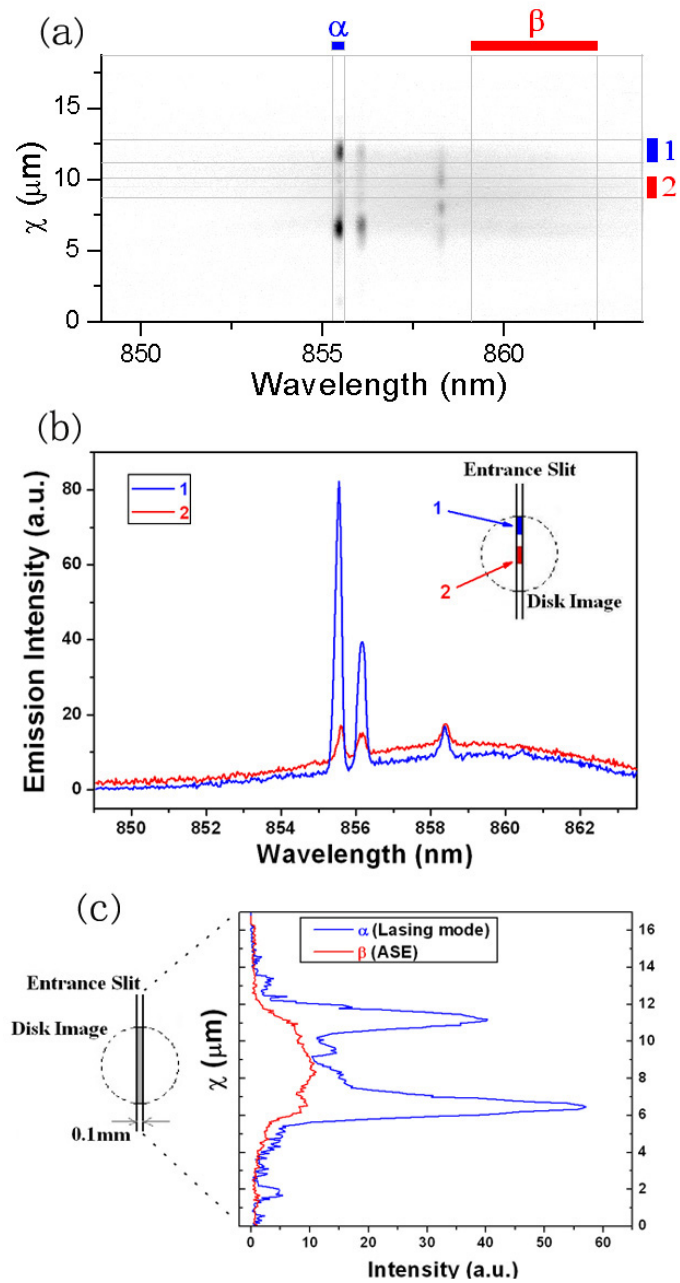


Fig. 6. (a) Two-dimensional spatial-spectral image of the emission from the microdisk in Fig. 2. The incident pump power is $44\mu\text{W}$. (b) Blue (red) curve is the spectrum of emission collected from the edge (center) part of the disk, corresponding to the horizontal strip marked by 1 (2) in (a). (c) Blue (red) line represents the emission intensity distribution across the disk diameter inside the vertical strip marked by α (β) in (a).

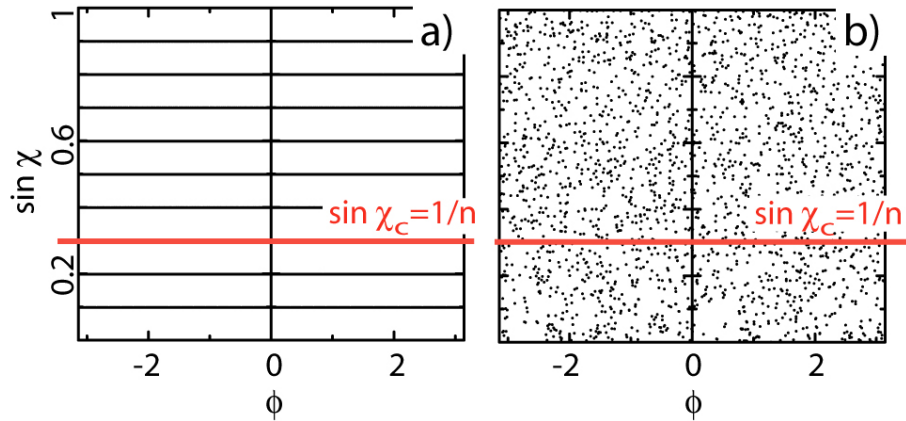


Fig. 7. Poincaré surface of section (SOS) in (a) a circular microcavity and (b) the microdisk of rough boundary shown in Fig. 2. Note the chaotic dynamics in the fabricated microcavity.

3. Theoretical description

To understand the dynamics inside the micro-resonator, it is necessary to consider the system behavior in the phase (coordinate – momentum) space. For almost-circular systems described here we use the polar system of coordinates, and represent trajectory in terms of polar angle ϕ and sine of angle of incidence χ , which is proportional to the angular momentum. We depict the classical dynamics of the system via Poincaré surface of section (SOS). To build SOS, we follow the ray trajectory started inside the system, and plot its position (ϕ) and angular momentum ($\sin \chi$) each time the trajectory hits the system, and plot its position (ϕ) and angular momentum ($\sin \chi$) each time the trajectory hits the system, and plot its position (ϕ) and angular momentum ($\sin \chi$) each time the trajectory hits the system. We then use the law of reflection to determine the dynamics after the “bounce”. Thus, the resulting picture represents the “stroboscopic” projection of the system motion onto 2D plane.

If the system has circular symmetry, the angular momentum $m\hbar$ of any trajectory is conserved, where $m = 2\pi nR/\lambda_0$ [7]. Correspondingly, each trajectory follows a 1D horizontal line in SOS. The line $\sin \chi = 1/n$ effectively separates the SOS into two parts. The trajectories which fall below this line can refractively escape from the system. The ones above the “critical line” are classically trapped inside by the total internal reflection. The corresponding modes of wave-dynamical system are allowed to escape the cavity only through exponentially suppressed evanescent leakage, thus have extremely high Q-factors [21].

Introduction of the boundary roughness dramatically changes the ray dynamics inside the system. Thus the stability of all WG trajectories inside the experimental device described in the previous section (corresponding to $\kappa \approx 0.2$) is completely destroyed (see Fig. 7). Furthermore, in the absence of circular symmetry, the angular momentum is no longer a conserved quantity, and the system becomes classically chaotic. As the ray propagates through such a cavity, its angular momentum undergoes the diffusive motion. No ray is now trapped above the “critical line”, which seemingly leads to the absence of high-Q modes.

However, the classical angular-momentum diffusion of the initially close ray trajectories may be suppressed by a destructive interference in wave-dynamical system. Such an effect is known as dynamical localization, which in some sense similar to Anderson localization of electrons in disordered potential; however, while the later takes place in the real (coordinate) space, the former takes place in the phase (momentum) space and is thus related to the system “propagation” (dynamics). The dynamical localization, initially introduced for a quantum analog of classically chaotic kicked-rotator [14], was later mapped onto the dynamics of quantum billiards [10] and semiclassical optical microcavities [18].

The real space structure of the optical mode formed as a result of dynamical localization somewhat resembles the WG mode of regular (circular) resonator. Thus, similarly to the standard WG modes most of the mode intensity is localized in an annular region along the boundary. However, as opposed to the standard WG patterns (see e.g. Fig. 1 in Ref. [11]), inside the annulus the mode of the rough resonator shows strong and irregular intensity fluctuations - see the inset of Fig. 8(a). Furthermore, while any WG wavefunction corresponds to some definite value of the angular momentum, the modes of the rough resonator shows the exponential distribution of different angular momentum components ψ_m , localized near some central angular momentum value m_0 :

$$\psi_m \propto \exp\left(-\frac{|m - m_0|}{l}\right), \quad (4)$$

where the parameter l , which defines the localization length (in the unit of angular momentum/ \hbar) is related to roughness parameter κ . Specifically, beyond the perturbative regime, i.e. when the condition in Eq. (2) is violated, $l \propto (nkR_0\kappa)^2$ with $k = 2\pi/\lambda_0$ [10]. We note that since DL as any statistical process is often accompanied by strong fluctuations [10, 22, 23] [see Fig. 8(b)], the Eq. (4) describes the envelope of the mode in the angular momentum representation.

Since the escape from the resonator is dominated by a portion of the mode having angular momenta below the critical value $m_c = 2\pi R_0/\lambda_0$ (corresponding to the angle of total internal reflection $\sin \chi_c = 1/n$), the quality parameter of the mode can be approximated using $Q \approx 1/\psi_{m_c}^2 \propto \exp[2(m_0 - kR_0)/l]$ [18]. Therefore, the dynamically localized mode with m_0 sufficiently above the critical line and small (in comparison with R_0/λ) localization length, may have relatively long lifetime, and can be used in all resonance-based systems (lasers, sensors, etc.).

When the localization length [10] $l \propto (\kappa nkR_0)^2$ becomes of the order of nkR_0 , the escape from the resonator is no longer strongly suppressed by dynamical localization, and the system no longer supports high- Q whispering-gallery modes – which sets an upper bound for the roughness for an optical microdisk resonator

$$\kappa \ll 1/\sqrt{nkR_0} \quad (5)$$

Note that in the semiclassical regime ($kR_0 \gg 1$) this criterion is much less stringent than the perturbative border (2).

We confirm the DL structure of the (experimentally observed) lasing mode described in the previous Section using the numerical calculation technique based on S -matrix method. In this approach, originally introduced in Ref. [24], and adopted for optical resonators in Ref. [18], the electromagnetic wave is represented by a series of circular waves converging to the center and diverging from it. The S -matrix itself defines the relation between these two series of waves. The solutions of the Maxwell equations correspond to the unit-eigenvalue eigenvector of the S -matrix, which provide the complete information about the real- and angular momentum-space representation of a given optical mode of the system (for the detailed description of this approach see Ref. [25]).

The lasing mode identified from our simulations is shown in Fig. 8. In order to eliminate the fitting parameters related to the finite resolution of the optical microscope used in our experiment, we compare the numerically calculated and experimentally measured angle-averaged intensities. The constant ASE background is subtracted from the measured intensity distribution at the lasing frequency. The comparison, shown in Fig. 8 confirms that the numerically simulated mode is in fact the one observed experimentally in Fig. 4, while its angular momentum representation confirms its dynamically localized character. The localization length $l \approx 12.4$

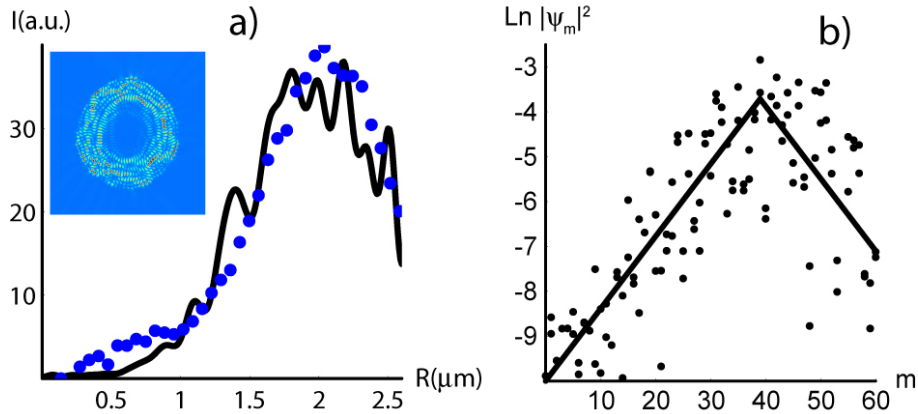


Fig. 8. (a) Angle-averaged radial structure of the mode obtained in numerical calculations (solid line) and in experiments (dots) (constant ASE background subtracted). the inset shows the real-space mode structure. (b) The angular-momentum distribution of the lasing mode obtained from our numerical simulations in logarithmic scale (dots) and its fit to exponential (solid lines).

obtained from our simulations is in a good agreement with the estimate for a rough billiard [10], and the theoretical value of the Q -factor for the lasing mode is 4.7×10^3 .

4. Conclusions

In conclusion, we have studied the effect of boundary roughness on the lasing modes in semiconductor microdisks. Despite classically chaotic ray dynamics, our experiments show lasing with decent threshold. We have demonstrated that the lasing modes in our devices originate from dynamical Anderson localization. Our results demonstrate that the microdisk resonators based on DL modes have a significant fabrication tolerance advantage over their “regular” counterparts.

Acknowledgments

The experimental work was supported by the MRSEC program of the National Science Foundation at the Materials Science Center of Northwestern University. The theoretical work was partially supported by NSF grants, and Princeton Institute for the Science and Technology of Materials (PRISM).